ARL-TR-9078 ● SEP 2020

DEVCOM ARMY RESEARCH LABORATORY

Examination of Biopolymer Electrodeposition with Functional Additives

by Jordan M Dreher, Jessica L Terrell, Deborah A Sarkes, Thomas H Segall-Shapiro, and Justin P Jahnke

NOTICES

Disclaimers

The findings in this report are not to be construed as an official Department of the Army position unless so designated by other authorized documents.

Citation of manufacturer's or trade names does not constitute an official endorsement or approval of the use thereof.

Destroy this report when it is no longer needed. Do not return it to the originator.

ARL-TR-9078 ● SEP 2020

Examination of Biopolymer Electrodeposition with Functional Additives

Jessica L Terrell, Deborah A Sarkes, Thomas H Segall-Shapiro, and Justin P Jahnke
Sensors and Electron Devices Directorate, CCDC Army Research Laboratory

Jordan M Dreher
Oak Ridge Associated Universities

REPORT DOCUMENTATION PAGE

Form Approved
OMB No. 0704-0188

1. REPORT DATE *(DD-MM-YYYY)*	2. REPORT TYPE	3. DATES COVERED (From - To)
September 2020	Technical Report	September 2019–September 2020

4. TITLE AND SUBTITLE
Examination of Biopolymer Electrodeposition with Functional Additives

5a. CONTRACT NUMBER

5b. GRANT NUMBER

5c. PROGRAM ELEMENT NUMBER

6. AUTHOR(S)
Jordan M Dreher, Jessica L Terrell, Deborah A Sarkes, Thomas H Segall-Shapiro, and Justin P Jahnke

5d. PROJECT NUMBER

5e. TASK NUMBER

5f. WORK UNIT NUMBER

7. PERFORMING ORGANIZATION NAME(S) AND ADDRESS(ES)
CCDC Army Research Laboratory
ATTN: FCDD-RLS-CB
Adelphi, MD 20783-1138

8. PERFORMING ORGANIZATION REPORT NUMBER
ARL-TR-9078

9. SPONSORING/MONITORING AGENCY NAME(S) AND ADDRESS(ES)

10. SPONSOR/MONITOR'S ACRONYM(S)

11. SPONSOR/MONITOR'S REPORT NUMBER(S)

12. DISTRIBUTION/AVAILABILITY STATEMENT
Approved for public release; distribution is unlimited.

13. SUPPLEMENTARY NOTES
ORCID ID(s): Jessica L Terrell, 0000-0002-7095-4198; Thomas H Segall-Shapiro, 0000-0001-9364-6537

14. ABSTRACT
Here we describe how electrodeposition of biopolymers can be used to prepare coatings incorporating additives to control interactions within the RF regime of the electromagnetic spectrum. Specifically, pH changes are used to drive the co-deposition of two polysaccharides (chitosan and alginate) and one proteinaceous material (silk) with one dielectric (strontium titanate) and two magnetic (permalloy and magnetite) additives that are relevant for RF materials. The resulting materials were freeze-dried and characterized using scanning electron microscopy to determine film structure and the uniformity of the additive distribution. It was determined that silk electrodeposition gave the best additive uniformity for both magnetic and dielectric additives.

15. SUBJECT TERMS
electrodeposition, silk, alginate, chitosan, radio-frequency, biofabrication, biopolymer

16. SECURITY CLASSIFICATION OF:			17. LIMITATION OF ABSTRACT	18. NUMBER OF PAGES	19a. NAME OF RESPONSIBLE PERSON
a. REPORT	b. ABSTRACT	c. THIS PAGE			Justin P Jahnke
Unclassified	Unclassified	Unclassified	UU	23	19b. TELEPHONE NUMBER (Include area code) (301) 394-0252

Contents

List of Figures

List of Tables

Acknowledgments

The authors would like to thank Professor David Kaplan of Tufts University for providing silk cocoons for processing into aqueous silk and for access to onsite facilities and equipment at Tufts University to execute this task in accordance with ARL CRADA JWS# 19-001-003. The authors would also like to thank Professors William Bentley, Gregory Payne, and their research groups at the University of Maryland for resources on biopolymer electrodeposition and help with chitosan dissolution under ARL CRADA JWS# 14-052-J008. Jordan Dreher acknowledges support from the Oak Ridge Associated University Fellowship under contract number W911NF1920334.

1. Introduction

The Army has increasing need for functional coatings where the distribution of the functional additive is more precisely and uniformly controlled to achieve the desired mix of functional properties while maintaining acceptable weight, cost, and mechanical properties.[1–2] In particular, coatings and films that interact with various regions of the electromagnetic (EM) spectrum are of considerable interest. In particular, coating properties within the RF region of the spectrum are controlled by the subwavelength distribution of functional dielectric and magnetite additives.[3–5] With recent advances in the areas of synthetic biology and bioengineering, there are increasing capabilities for assembling biological components into complex materials (i.e., biofabrication).[6–8] Correspondingly, there is the increasing possibility of using tailored biomaterials to meet Army needs, with biology either providing the functionality or enabling the assembly of a functional additive. For example, there has been some precedent to guide the assembly of nanoparticles within biopolymer scaffolds[9] and it is becoming increasingly feasible to develop genetically engineered biomaterial variants that have specific affinity handles incorporated to further enhance the precision of assembly.[10–13] However, development of processing methods for specific coating applications is often lacking.

Here we look at methods for biopolymer electrodeposition to incorporate functional nanoparticles via entrapment within the biopolymer scaffold and to examine the ability to control spatial distribution through layering. By controlling the nanoparticle assembly, we reduce the amount of nanoparticle loading needed, thereby reducing weight, and potentially, the cost. The initial application for these biomaterial films targets conformal antenna materials for the RF spectrum, which require the introduction of dielectric and magnetic properties (Fig. 1).

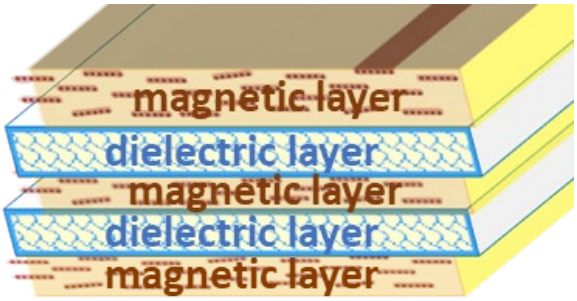

Fig. 1 Schematic of an example assembly of interest for RF-active coatings

Electrodeposition uses an electrochemical potential to drive an oxidation–reduction reaction that causes the formation of a solid on the electrode surface. The electrode

can directly oxidize or reduce the material to be precipitated, but in the case of biopolymer precipitation, it is also common to use the electrode to drive a pH change that then causes the gelation of a stimuli-responsive biopolymer to form a hydrogel. The hydrogel can then either be freeze-dried or supercritically dried to form a porous foam with a preserved structure, or alternatively, dried near ambient conditions to deliberately densify the hydrogel as water evaporates to result in a dense, thin film.[14] Biopolymers that have been reported to undergo a pH-driven sol-gel transition via electrodeposition include chitosan,[15–16] alginate,[17] and silk,[18–19] among others.

Electrodeposition has some advantages over alternative approaches to form gels and films. Typically, the film quality is uniform and the thickness is also well controlled by regulating the amount of charge introduced by the electrode as well as the solution conditions.[20] Unlike spin-coating, the excess solution is not lost during processing. Like layer-by-layer deposition, it is possible to move the electrode between two baths to introduce distinct layers, with electrodeposition being well suited to materials where layer thicknesses on the order of microns to millimeters are desired.[21] Furthermore, it is possible to vary the current at the electrode over time to change the local morphology or introduce layering without the need to switch baths.

Here, two polysaccharides (chitosan and alginate) and one proteinaceous material (silk) were examined for their ability to form electrodeposited films with one dielectric (strontium titanate [$SrTiO_3$]) and two magnetic (permalloy and magnetite [Fe_3O_4]) additives that are relevant for RF materials. Scanning electron microscopy (SEM) characterization of the resulting materials was used to examine the uniformity of the distribution and entrapment of the particles within the biomaterials as well as characterize film porosity and thickness.

Table 1 summarizes the samples synthesized in the three scaffolds. Chitosan is a positively charged polysaccharide derived from the hard outer skeleton of shellfish. It is biodegradable, nontoxic, and antibacterial.[15,21–22] Chitosan was also used to develop the setup that was employed with the other materials and test the ability of electrodeposition to drive the formation of layers. Alginate is a negatively charged polysaccharide whose solubility can be mediated by pH-driven change in the presence of calcium carbonate ($CaCO_3$), in which it is soluble. Silk fibroin can be dissolved from silkworm silk and then gelled as a result of pH changes. All three materials resulted in mostly porous films upon freeze-drying, with different extents of uniformity for the additive incorporated. Silk gave the best additive uniformity, and Fe_3O_4 was in general the most challenging additive to incorporate uniformly, with $SrTiO_3$ dispersing most readily.

Table 1 Summary of the samples characterized in this report

Figure	Solution	Surface area (mm^2)	Additives (mg/ml)	Current density	Time	Thickness (microns)
2	0.75% chitosan	A. 96 B. 128 C. 4.85	N/A	A. 1 A/m^2 B. 2 A/m^2 C. 15.8 A/m^2	A. 2 h (coil counter) B. 2 h C. 30 s on, 5 s off; 10 cycles	A. 69 B. 176 C. 20
3	0.75% chitosan	128	5	8 A/m^2	5 min	A. 38–145 B. 118–202 C. 110 D. 97
4	A. 1% chitosan B. 0.75% chitosan	128	100	15.8 A/m^2	30 s on, 5 s off A. 5 cycles B. 10 cycles	A. 291 B. 70
5	1% sodium alginate, 0.5% $CaCO_3$ (film submerged in 0.1 M $CaCl_2$)	128	N/A	3 A/m2	10 min	720
6	2.6% silk	128	5	3 V (voltage controlled)	3 min	A. 173 B. 27–57 C. 9.1

Note: $CaCO_3$ = calcium carbonate; $CaCl_2$= calcium chloride.

2. Experimental

2.1 Electrodeposition

All electrodepositions were performed using a Biologic VL3 8 channel potentiostat. The working and counter electrodes were typically gold surfaces that had been deposited onto silicon wafers; the wire electrode setup used a titanium wire working electrode. A silver/silver chloride reference electrode was used. For the wire electrode measurements, a glass vial was used to house the electrodes and deposition solution. For other electrode setups, a 128-mm^2 silicone mold was prepared using the Sylgard 184 formulation to conserve solution and ensure reproducible areas. A 1:10 mixture was prepared in a plastic petri dish, degassed, and allowed to cure in the incubator overnight. Wells were cut out with a scalpel, with an area of 128 mm^2 used in the case of the horizontal setup. The electrodeposition setups are shown in Fig. 2, along with the preparation of the mold (Fig. 2A) and an example of a resulting film (Fig. 2E). The deposition currents were controlled using chronopotentiometry experiments. Solution composition and current densities were selected to be consistent with literature values and are noted in Section 3.

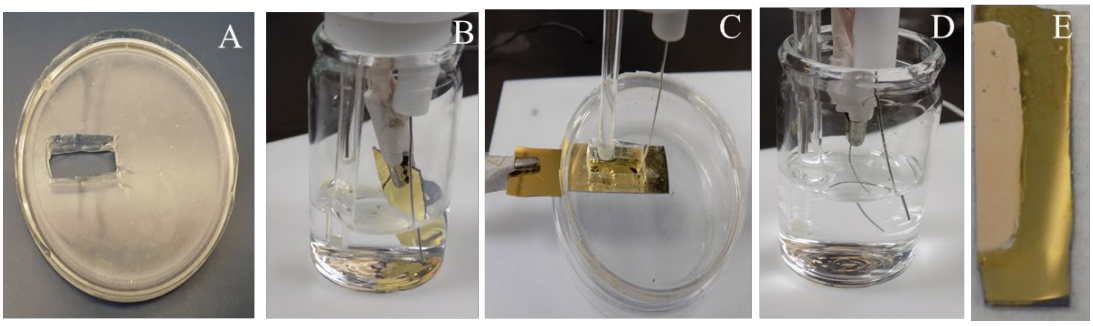

Fig. 2 A) Polydimethylsiloxane (PDMS) mold: A mixture of 1:10 ratio of elastomer to base was mixed in a plastic petri dish (diameter of 53 mm), degassed, and allowed to cure in the incubator overnight. A 128-mm^2 well was cut out with a scalpel. B) Vertical electrodeposition setup where all electrodes are dipped into the chitosan solution. C) Horizontal electrodeposition setup where the chitosan solution is placed on top of the working electrode. This is done with the well cut from PDMS and with counter and reference electrodes dipped into the solution, refraining from touching the working electrode. D) Wire electrodeposition solution with all electrodes dipped into the chitosan solution. E) Example film formed using the electrodeposition approach.

2.2 Postprocessing

After deposition, the films were typically frozen in liquid nitrogen and then dried in a Labconco FreeZon 2.5 Plus lyophilizer. Without any additives, the films were translucent gels before freezing and lyophilization, and were brittle and opaque after drying. As an alternative to freeze-drying, in some cases, the films were allowed to dry under ambient conditions, in which case a thin, translucent film remained.

2.3 Characterization

SEM was the primary experimental technique used to characterize the electrodeposited films. A Quanta 200F SEM was used operating in high vacuum and at 5 or 10 kV. Cross-sectional views were obtained by scribing and fracturing the wafers. Thicknesses were measured near the center of the sample, where possible.

3. Results and Discussion

A number of setups have been used for electrodeposition of chitosan in the literature. Planar electrodes can be used either horizontally or vertically. Furthermore, wire electrodes have been used to deposit cylinders of materials[21] with distinct layers being introduced by varying the current over time. All three setups were tested to determine the best setups for examining other biopolymers and electrochemical additives.

The films formed by the three setups were freeze-dried, fractured, and examined using SEM to analyze the morphology and reproducibility of the materials. Representative SEM images for the three setups are shown in Fig. 3. Figure 3A shows a cross-sectional image of a film deposited in the vertical setup using a 0.75% chitosan solution. The film was electrically deposited onto the gold electrode (96-mm^2 surface area) at a current density of 1 A/m^2 for 2 h. The film had a measured thickness of 70 μm. The structure of the film was porous, with some variability in the size of the pores.

Figure 3B shows a similar cross-sectional image for a film deposited in the horizontal setup. Again, a 0.75% chitosan solution was electrically deposited onto the gold electrode (128-mm^2 surface area), but the current density was 2 A/m^2 and the time 2 h. The film had a measured thickness of 90 μm. Overall, the results are similar to the vertical setup, but there appears to be some increase in the porosity of the film and less variation in the size of the pores. There seems to be a separating line toward the bottom of the film, which is thought to be a result of contraction while drying. In addition to these differences apparent in the SEM images, the horizontal films also showed greater uniformity across the deposition area.

Figure 3C shows the results for a titanium wire deposition using a 0.75% chitosan solution at 15.8 A/m^2 for 10 cycles of 30 s on, 5 s off. Similar results were obtained for other cycle lengths and no difference in layer thickness with cycle length was observed. Layers ranged in thickness from 6 to 11 μm. These values are slightly lower than the literature value of 20 μm for the same current density and deposition time.[21] This may be due to the fact that the solution used in the literature also contained hydrogen peroxide and sodium chloride. The deposition was uneven across the surface of the wire as some areas were not covered in film, but there was evidence of a porous layered structure resulting from the difference in the on/off cycles. Although there was variability in pore size within the horizontal setup, the overall thickness and reproducibility of the films was greater than that of the other methods. Based on these results, the horizontal setup was selected for further study with additive incorporation.

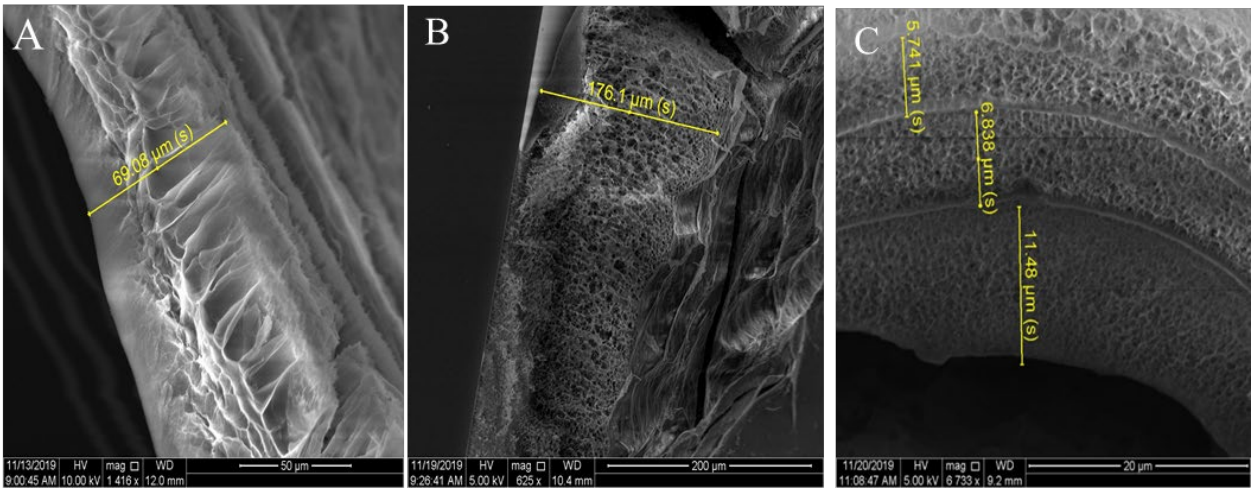

Fig. 3 Comparison of chitosan films using various electrodeposition configurations. Cross sections of electrodeposited films are shown by SEM images for the A) vertical setup B) horizontal setup, and C) wire setup.

Different extents of incorporation were observed when the three additives were incorporated into the electrodeposited chitosan films using the horizontal setup. Representative SEM images for the films are shown in Fig. 4. All films were formed with a 0.75% chitosan solution run at 8 A/m^2 (surface area of 128 mm^2), for 5 min, freeze-dried, fractured, sputter-coated with 5 nm of gold, and examined using SEM to analyze the morphology and reproducibility of the materials. Figure 4A shows the cross-sectional images of the electrodeposited chitosan control without particles at approximately the thinnest and thickest regions of the film. In both areas, the pore size was relatively uniform, but thickness of the film varied between 38 and 150 µm depending on the region of the film.

Figure 4B shows the cross-sectional image of the electrodeposited chitosan with Fe_3O_4 nanoparticles. The thickness of the film varied between 120 and 200 µm depending on the region of the film. The pore structure is altered compared to the control film (Fig. 4A), with larger pores and a more open structure observed. There is also uneven dispersal of the nanoparticles. There are a significant number of larger aggregates of Fe_3O_4 that partially disrupt the chitosan structure. The large aggregates may be due at least in part to incomplete dispersal in solution prior to electrodeposition. However, many particles are also dispersed individually or in small aggregates along the chitosan platelets; these two types of nanoparticle environments are highlighted by arrows in the figure.

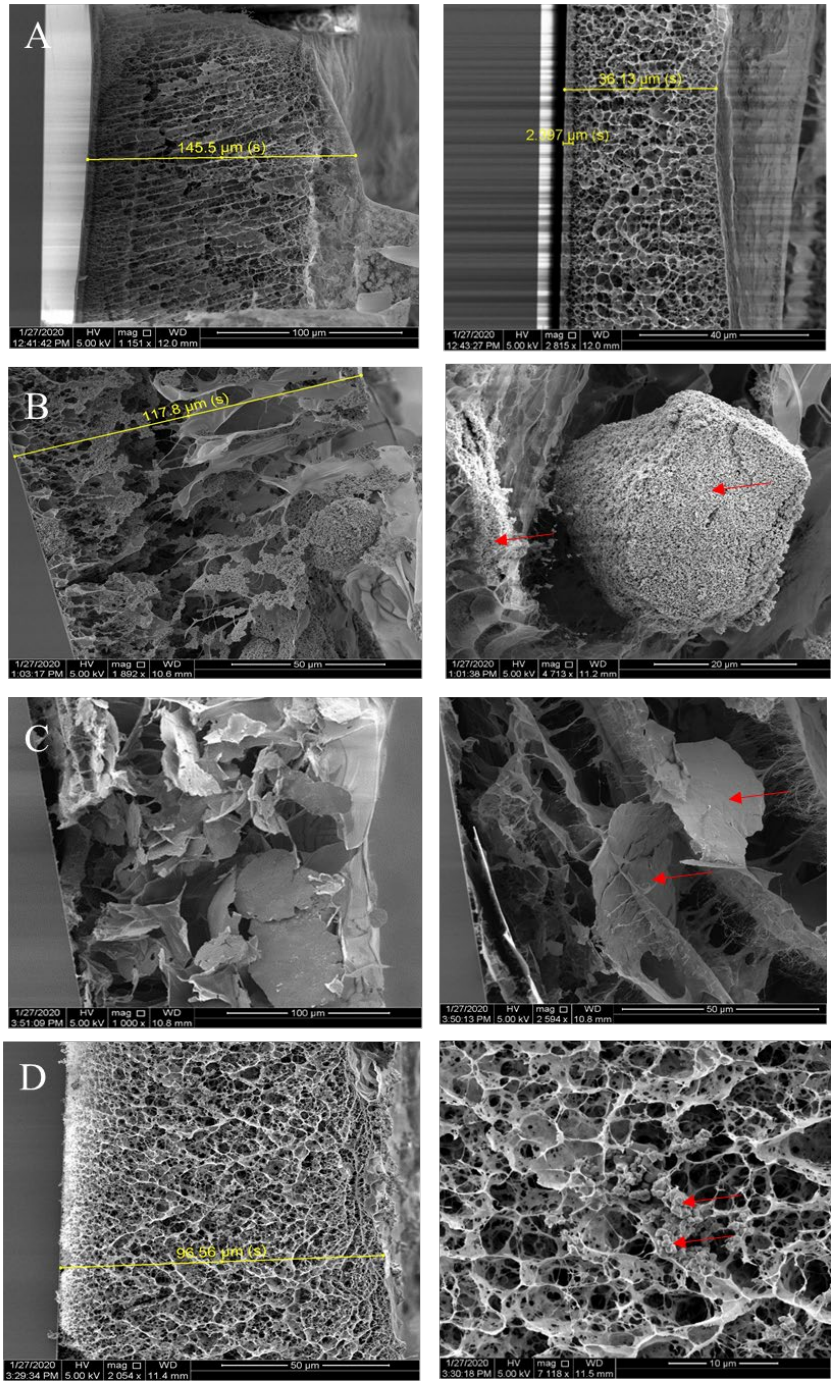

Fig. 4 SEM images of cross sections of the electrodeposited films of either A) chitosan control without particles or with 5 mg/mL of B) Fe_3O_4, C) permalloy, or D) $SrTiO_3$. Arrows indicate the locations of particles. Two images showing different regions of the films are included.

Figure 4C shows the cross-sectional image of the electrodeposited chitosan with permalloy flakes. The film had a thickness of about 110 µm based on the scale bar. The permalloy flakes are much larger than either the approximately spherical Fe_3O_4

or $SrTiO_3$ nanoparticles and are again highlighted by arrows. Nonetheless, it disperses fairly uniformly within the films. However, the density of the flakes does vary between different regions of the film, as shown in the two SEM images.

Figure 4D shows the cross-sectional image of the electrodeposited chitosan with $SrTiO_3$ nanoparticles. The film had a measured thickness of 97 μm. The pore structure of the film was very similar to the control films, despite the addition of the $SrTiO_3$. The particles are also mostly dispersed on the chitosan scaffold, but the density is not high enough to uniformly coat the scaffold. Regions of particle incorporation are shown by arrows. From these results, it is clear that the various particles behave differently when deposited with the chitosan and furthermore alter the pore structure of the chitosan film, with the $SrTiO_3$ disrupting the structure the least.

One advantage of electrodeposition is that by controlling the current or voltage over time, the deposition profile can, in principle, be altered. This is possible not only in wire setups as shown in Fig. 2D, but also in the planar horizontal setup (Fig. 2C). A similar deposition protocol was used; the films formed with chitosan solutions were run at 15.8 A/m^2 for 30 s on, 5 s off (surface area of 128 mm^2). After film formation, the material was freeze-dried, fractured, and examined using SEM to analyze the morphology and reproducibility of the materials. To investigate how an additive affects the layering process, Fe_3O_4 was also included in some depositions. Representative SEM images are shown in Fig. 5. Figure 5A shows the cross-sectional image of the electrodeposited, layered chitosan without any additives. The film was made with 1% chitosan and run for 5 cycles. It had a total thickness of 290 μm. The layers formed as a result of switching between on and off times, but varied in thickness. Layer thickness ranged from 45 to 72 μm. These thicknesses are greater than observed with the wire setup, but may be due to the differences in geometry; the cylindrical geometry of the wire results in increasing differential volumes as ions diffuse away from the electrode, which does not occur with planar electrodes.

As with the unilayer deposition, the Fe_3O_4 particles do not fully disperse in the chitosan film. Figure 5B shows the cross-sectional image of the electrodeposited, layered chitosan with the addition of Fe_3O_4 nanoparticles. The film was made with 0.75% chitosan with 100 mg/ml of Fe_3O_4 and run for 10 cycles. The structure of the film was somewhat porous with unevenly dispersed particles as there are small and large aggregates of Fe_3O_4 shown. Despite the increase in the number of cycles relative to the control without Fe_3O_4, the film had an overall measured thickness of only 70 μm and furthermore only a handful of layers are observed. The layers that are present are relatively uniform in thickness (25 μm), although the large aggregates lead to disruptions in the layers. Overall, these results show the

possibility of using layering in these systems, but considerable work remains to be done both on dispersal of the particles and understanding how the presence of the additive affects layer formation and thickness.

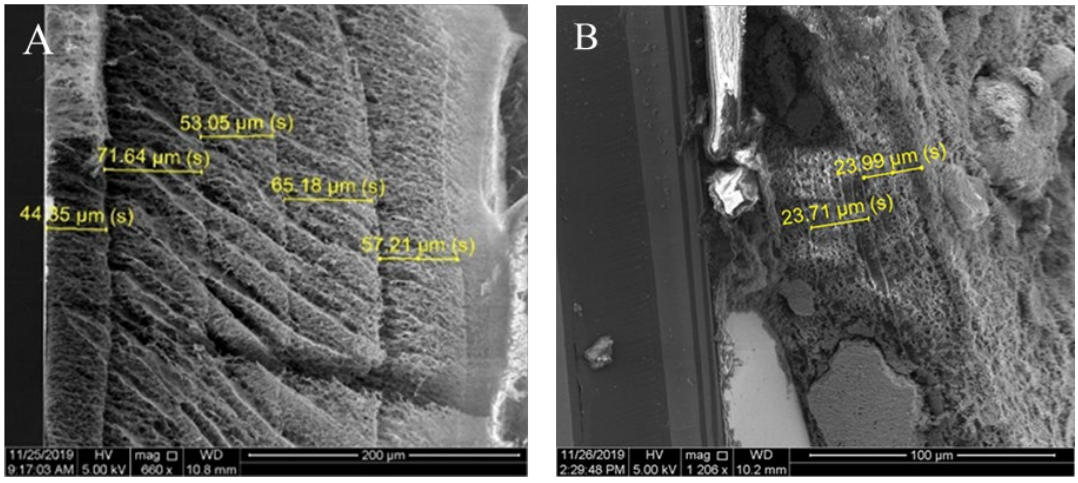

Fig. 5 Cross-sectional SEM images of electrodeposited layered films with A) chitosan and B) chitosan with Fe_3O_4

Beyond chitosan, other biopolymers, including silk and sodium alginate, can be deposited using similar methods. The negative charge of sodium alginate contrasts with the positive charge of chitosan, while silk is a proteinaceous material, which gives it a complex chemistry that can be further altered by genetic engineering. To examine how readily the electrodeposition setup for chitosan generalized, both of these materials were interrogated as well.

While sodium alginate and chitosan are both polysaccharides, the mechanism of the deposition is different. Alginate electrodeposition depends on a pH change driving a change in the solubility of $CaCO_3$. The calcium cations, being divalent, serve as physical crosslinks for the alginate gel. The film was formed with a 1% sodium alginate and 0.5% $CaCO_3$ solution run at 3 A/m^2 for 10 min (surface area of 128 mm^2), freeze-dried, fractured, sputter coated with 5 nm of gold, and examined using SEM to analyze the morphology and reproducibility of the materials. A representative cross-sectional image of the electrodeposited alginate is shown in Fig. 6. The film had a measured thickness of 720 µm. This value is thicker than literature values due to the longer time of deposition, but similar to the expected trends. A linear extrapolation of the literature values would give an expected thickness of 830 µm for the same current density and solution percentage.[17] The structure of the film appears to be denser than the chitosan films, although remaining porous. Although the resulting structure is not as porous as chitosan, these results support the idea that the electrodeposition method used for chitosan can also be applied to other materials such as alginate.

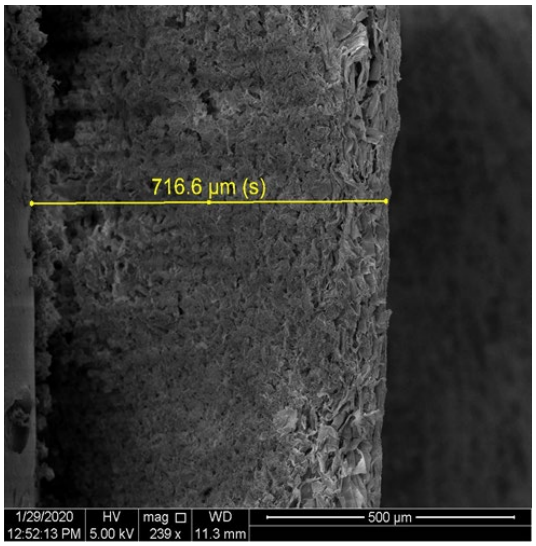

Fig. 6 Cross-sectional SEM image of an alginate film

Silk gelation can also be induced by an electrochemically driven pH change, and this mechanism was investigated for its ability to incorporate functional additives. Representative SEM images are shown in Fig. 7. All films were formed with a 2.6% silk solution run at 3 V for 3 min (surface area of 128 mm^2), freeze dried, fractured, sputter coated with 5 nm of gold, and examined using SEM to analyze the morphology and reproducibility of the materials. Figure 7A shows the cross-sectional image of the electrodeposited silk control without any particles. The film had a measured thickness of 170 µm. Silk gels reported in the literature generally reach millimeter to centimeter thicknesses in less than 3 min,[19] so the thickness observed here is much lower than expected. The most likely reasons are related to the removal from the electrode surface and the drying process. The gels are not mechanically robust before drying, and this may lead to the loss of material, in addition to some contraction upon drying. The structure of the freeze-dried film was string-like and fibrous.

Figure 7B shows the cross-sectional image of the electrodeposited silk with Fe_3O_4 nanoparticles. The film had a varying thickness of 27 to 57 µm depending on the region of the film. The structure of the film was fibrous, and, at least when compared to the Fe_3O_4-chitosan films, the Fe_3O_4 particles are more uniformly distributed in the film, even if a fully uniform dispersal is not achieved.

Figure 7C shows the cross-sectional image of the electrodeposited silk with $SrTiO_3$ nanoparticles. The film had a measured thickness of 9 µm, perhaps due to extensive compaction during drying. The structure of the film was less porous but had a uniform dispersal of the $SrTiO_3$ particles. These results support the idea that the electrodeposition method used for chitosan can also be applied to other materials,

such as silk, even with the addition of nanoparticles. Promisingly, more uniform distributions of the particles are observed, suggesting that further investigation of silk electrodeposition would be a fruitful avenue to pursue.

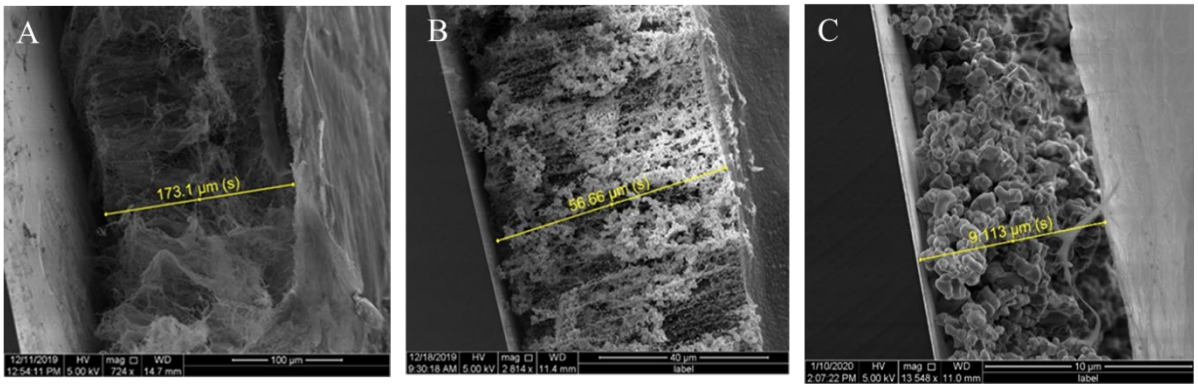

Fig. 7 Cross-sectional SEM images of electrodeposited silk films A) without particles, B) with 5 mg/ml of Fe_3O_4, and C) with 5 mg/ml of $SrTiO_3$

4. Conclusion

Several biomaterials were investigated for their ability to be electrodeposited while incorporating EM functional nanoparticles. Chitosan can be electrodeposited to form uniform and porous thin films, with or without layers, and in different orientations. To various extents, this structure is disrupted by the addition of nanoparticles. In particular, Fe_3O_4 did not incorporate well and also disrupted the layered structure when added. More uniform distributions were achieved with permalloy and $SrTiO_3$, but there was still some aggregation and both also altered the pore structure of the material. A preliminary investigation of alginate and silk as alternative scaffold materials was conducted, and the silk in particular appears to be a promising material for further study. While it experienced some changes to the film porosities, a more uniform distribution of the two additives examined was observed. In the silk in particular, where the films as gelled are quite fragile, there is the potential to introduce chemical cross-links through the tyrosine residues as a postprocessing step to improve mechanical toughness and stiffness. Longer-term goals include genetically engineering the silk to incorporate amino acid residues that promote an affinity between the silk and the additives.

5. References

1. Lazarus N, Bedair SS. Improved power transfer to wearable systems through stretchable magnetic composites. Appl Phys A. 2016;122(5).

2. Huitema L, Reveyrand T, Mattei J-L, Arnaud E, Decroze C, Monediere T. Frequency tunable antenna using a magneto-dielectric material for DVB-H application. IEEE Trans Antennas Propag**.** 2013;61(9):4456-4466.

3. Luo S, Shen Y, Yu S, Wan Y, Liao W-H, Sun R, Wong C-P. Construction of a 3D-$BaTiO_3$ network leading to significantly enhanced dielectric permittivity and energy storage density of polymer composites. Energy Environ Sci. 2017;10(1):137–144.

4. Karilainen AO, Ikonen PMT, Simovski CR, Tretyakov SA, Lagarkov AN, Maklakov SA, Rozanov KN, Starostenko SN. Experimental studies on antenna miniaturisation using magneto-dielectric and dielectric materials. IET Microw Antennas Propag. 2011;5(4):495–502.

5. Ikonen PMT, Rozanov KN, Osipov AV, Alitalo P, Tretyakov SA. Magnetodielectric substrates in antenna miniaturization: potential and limitations. IEEE Trans Antennas Propag. 2006;54(11):3391–3399.

6. Min K, Umar M, Seo H, Yim JH, Kam DG, Jeon H, Lee S, Kim S. Biocompatible, optically transparent, patterned, and flexible electrodes and radio-frequency antennas prepared from silk protein and silver nanowire networks. RSC Advances. 2017;7(1):574–580.

7. Heveran CM, Williams SL, Qiu J, Artier J, Hubler MH, Cook SM, Cameron JC, Srubar WV. Biomineralization and successive regeneration of engineered living building materials. Matter. 2020;2(2):481–494.

8. Gilbert C, Ellis T. Biological engineered living materials: growing functional materials with genetically programmable properties. ACS Synth Biol. 2019;8(1):1–15.

9. Li Y, Liu y, Gao T, et al. Self-assembly with orthogonal-imposed stimuli to impart structure and confer magnetic function to electrodeposited hydrogels. ACS Appl Biomats Interfaces. 2015;7(19). https://pubs.acs.org/doi/pdfplus/10.1021/acsami.5b02339.

10. Adams BL, Finch AS, Hurley MM, Sarkes DA, Stratis-Cullum DN. Genetically engineered peptides for inorganics: study of an unconstrained bacterial display technology and bulk aluminum alloy. Adv Mater 2013;25(33):4585–4591.

11. Dong H, Sarkes DA, Rice JJ, Hurley MM, Fu AJ, Stratis-Cullum DN. Living bacteria–nanoparticle hybrids mediated through surface-displayed peptides. Langmuir. 2018;34(20):5837–5848.

12. So CR, Hayamizu Y, Yazici H, Gresswell C, Khatayevich D, Tamerler C, Sarikaya M. Controlling self-assembly of engineered peptides on graphite by rational mutation. ACS Nano. 2012;6(2):1648–1656.

13. Solis DJ. Biological scaffolds for the peptide-directed assembly of nanoscale materials and devices. Cambridge (MA): Massachusetts Institute of Technology; 2006.

14. Guo C, Li C, Mu X, Kaplan DL. Engineering silk materials: From natural spinning to artificial processing. Appl Phys Rev. 2020;7(1):011313.

15. Zhao D, Yu S, Sun B, Gao S, Guo S, Zhao K. Biomedical applications of chitosan and its derivative nanoparticles. Polymers (Basel). 2018;10(4).

16. Cheng Y, Luo X, Betz J, Buckhout-White S, Bekdash O, Payne GF, Bentley WE, Rubloff GW. In situ quantitative visualization and characterization of chitosan electrodeposition with paired sidewall electrodes. Soft Matter. 2010;6(14):3177.

17. Cheng Y, Luo X, Betz J, Payne GF, Bentley WE, Rubloff GW. Mechanism of anodic electrodeposition of calcium alginate. Soft Matter. 2011;7(12):5677–5684.

18. Lin Y, Wang S, Chen Y, Wang Q, Burke KA, Spedden EM, Staii C, Weiss AS, Kaplan DL. Electrodeposited gels prepared from protein alloys. Nanomedicine (Lond). 2015;10(5):803–14.

19. Maniglio D, Bonani W, Bortoluzzi G, Servoli E, Motta A, Migliaresi C. Electrodeposition of silk fibroin on metal substrates. J Bioact Compat Pol. 2010;25(5):441–454.

20. Liu Y, Zhang B, Gray KM, Cheng Y, Kim E, Rubloff GW, Bentley WE, Wang Q, Payne GF. Electrodeposition of a weak polyelectrolyte hydrogel: remarkable effects of salt on kinetics, structure and properties. Soft Matter. 2013;9(9):2703.

21. Yan K, Ding FY, Bentley WE, Deng HB, Du YM, Payne GF, Shi XW. Coding for hydrogel organization through signal guided self-assembly. Soft Matter. 2014;10(3):465–469.

22. Gordonov T, Liba B, Terrell JL, Cheng Y, Luo X, Payne GF, Bentley WE. Bridging the bio-electronic interface with biofabrication. J Vis Exp. 2012;(64):e4231.

List of Symbols, Abbreviations, and Acronyms

$CaCl_2$	calcium chloride
$CaCO_3$	calcium carbonate
EM	electromagnetic
Fe_3O_4	magnetite
RF	radio frequency
SEM	scanning electron microscopy
$SrTiO_3$	strontium titanate

1 (PDF)	DEFENSE TECHNICAL INFORMATION CTR DTIC OCA
1 (PDF)	CCDC ARL FCDD RLD DCI TECH LIB
4 (PDF)	CCDC ARL FCDD RLS CB J JAHNKE D SARKES T SEGALL-SHAPIRO J TERRELL
1 (PDF)	J DREHER